Structure and properties of defects in amorphous silica: new insights from embedded cluster calculations

2005 J. Phys.: Condens. Matter 17 S2115

(http://iopscience.iop.org/0953-8984/17/21/007)

INSTITUTE OF PHYSICS PUBLISHING JOURNAL OF PHYSICS: CONDENSED MATTER

J. Phys.: Condens. Matter **17** (2005) S2115–S2140 doi:10.1088/0953-8984/17/21/007

Structure and properties of defects in amorphous silica: new insights from embedded cluster calculations

Peter V Sushko, Sanghamitra Mukhopadhyay, Andrey S Mysovsky, Vladimir B Sulimov, Adrian Taga and Alexander L Shluger[1]

Department of Physics and Astronomy, University College London, Gower Street, London WC1E 6BT, UK

E-mail: a.shluger@ucl.ac.uk

Received 10 February 2005, in final form 21 March 2005
Published 13 May 2005
Online at stacks.iop.org/JPhysCM/17/S2115

Abstract

We briefly review some of the approaches which have been used to study the distributions of defect properties in amorphous silica and focus mainly on the implementation of the embedded cluster method. We illustrate some of the results obtained using this method and discuss the remaining problems using the example of oxygen vacancy defects in amorphous SiO_2. The neutral vacancies are characterized by a wide distribution of formation energies and structural parameters. Our modelling predicts the two major structural kinds of positively charged vacancies (E′ centres): dimers and dangling bond centres. The local structure for both kinds of centres depends on the medium range structure of the surrounding amorphous network. We found that the majority of the dangling bond centres are unpuckered. The optical spectra and electron paramagnetic resonance parameters calculated for all defects are in good agreement with experimental data. The structural criteria which favour the formation of different kinds of centres in the original amorphous structure are formulated in terms of the average Si–O distance of oxygen ion with its two neighbouring silicon ions.

(Some figures in this article are in colour only in the electronic version)

1. Introduction

Amorphous silica is commonly used in the cores of optical fibres and is an integral part of most silicon-based metal–oxide–semiconductor devices. Due to its broad technological applications, it is one of the best studied amorphous materials [1, 2]. However, theoretical

[1] Author to whom any correspondence should be addressed.

modelling of the effects of structural disorder on defect properties and the relative abundance of different defect configurations in amorphous silica is only just starting to develop, in spite of a long history of defect studies [3–6]. We have been developing a method for predicting and analysing defect structures in a-SiO_2 based on an embedded cluster method. The purpose of this paper is to critically review the scope of application of this technique by means of selected examples based on studies of the structure and spectroscopic properties of oxygen vacancies in amorphous silica.

A common model of amorphous silica is that of a continuum random network where the crystalline connectivity is preserved and the geometric parameters are distributed in certain ranges (see, for example, [7] for discussion). Already at this simplified level, modelling defects in amorphous materials requires considering not only one or a few sites, as in crystals, but instead a statistical ensemble of structural sites. One then expects that defects would look similar to their analogues in the crystalline structure, but with statistically distributed parameters. Indeed, the recent theoretical studies of some defects, such as peroxy linkage species [3] and interstitial oxygen molecules [5] have demonstrated that their structures in α-quartz and in amorphous silica should be qualitatively very similar. The dependence of formation energies, structural parameters, diffusion barriers and spectroscopic parameters of these defects on details of the local and medium range environment can be characterized theoretically by statistical distributions (see, for example, [3]). However, experimentally these defects have been observed only in amorphous silica and the parameters of these distributions are very difficult to verify experimentally for several reasons discussed below.

Some of the problems related to studying the effect of disorder on the structure and properties of defects can be highlighted by another example: the neutral oxygen vacancy (NOV) in silica. This defect is believed to exist in both crystalline quartz and in most types of amorphous silica [8, 9]. However, it is diamagnetic and manifests itself mainly through the characteristic optical absorption peak and some possible transformations into other defects [8, 10, 11]. Therefore the effect of disorder is buried in the shape of the absorption spectrum and is not very easy to expose. Besides, NOV produced during the growth of thermal oxide or due to sample irradiation or via breaking Si–H bonds may occupy different sites in the amorphous network and thus again have different properties.

The family of positively charged oxygen vacancies, known as E′ centres, in crystalline and amorphous SiO_2 provides a different set of examples. These defects are paramagnetic and some of them have been assigned optical absorption bands. This makes them convenient for comparing the properties of defects in crystalline and amorphous environments. In particular, in a series of works Weeks and Nelson [12], Silsbee [13] and Jani *et al* [14] established with high precision all the strong and weak hyperfine interactions, including directions for the principal values of the E'_1 centre in α-quartz. The prevailing model of this defect, pioneered by Rudra and Fowler [15], is shown in figure 1(a). It is considered to be a positively charged oxygen vacancy which adopts a so-called puckered configuration (PC). Here the Si atom of the shorter Si–O bond (Si_S) accommodates an unpaired electron on a dangling bond whereas the silicon on the longer Si–O bond (Si_L) relaxes through the plane of its three neighbouring oxygen atoms and forms a bond with the oxygen 'back' atom, O_B in figure 1(a). Allan and Teter were the first to demonstrate that along with the PC, there is the dimer configuration (DC) (see figure 1(b)), wherein the two silicon atoms that face the vacancy relax very little from their ideal positions in the perfect quartz lattice [16]. Most calculations predict the PC to be lower in energy than the DC [17–20] and there is no clear experimental evidence that the DC is significantly populated in α-quartz.

It should be noted that recent calculations of the negative-U property of E'_1 centres in α-quartz [21] suggest that a pair of E'_1 centres is unstable with respect to a transformation

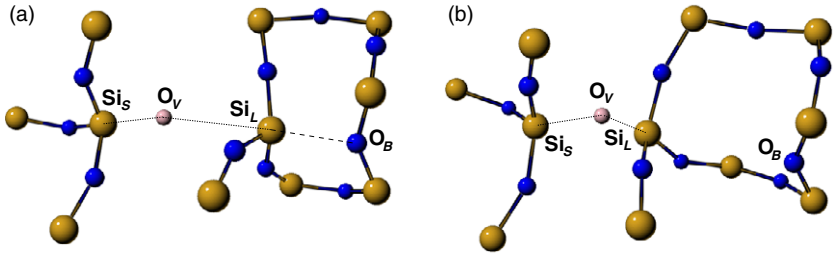

Figure 1. Two configurations of the E'_1 centre in α-quartz: (a) a puckered configuration and (b) a dimer configuration. In (a) Si_L (the Si atom of the longer Si–O bond) is puckered and makes a bond with an oxygen ion (O_B), Si_S (the Si of the shorter Si–O bond) carries the unpaired electron. O_V marks the oxygen vacancy site.

into a neutral oxygen vacancy and a doubly charged positive vacancy. These results imply that E'_1 centres cannot be formed at high concentrations when the charge transfer between the vacancies becomes effective. The same work [21] offers alternative models for paramagnetic centres in α-quartz.

In contrast to the α-quartz one, several atomistic models have been proposed for E′ centres in amorphous silica mainly detected using EPR [22–24]. The main component of this centre is a silicon dangling bond with an unpaired electron, which can exist on its own as a neutral defect, as a part of a positively charged oxygen vacancy (as in figure 1) or in an even more complex defect. These defects are labelled with subscripts α, β, γ, δ to distinguish species characterized by different EPR parameters (see, for example, the review [22]). However, their structural models are still controversial. For example, there are at least four different models of E'_δ centres [25–28]. The existence of topologically different E'_γ centres in γ-irradiated silica has recently been suggested on the basis of the analysis of fine features in the EPR spectra [29, 30]. Several other models of paramagnetic 'oxygen deficient' and 'silicon dangling bond' centres have been proposed in theoretical simulations [4, 6, 27, 31–33].

Experimentally, EPR signals attributed to different centres have been shown to coexist in some of the samples [22]. However, the relative concentrations of different centres depend on the details of sample preparation, the presence of impurities (e.g. H, F, Cl, P) and the method of irradiation (e.g. photons, electrons, high energy ions [34, 35] and neutrons [10]).

Finally, there exists a range of defects, such as self-trapped holes [36–38], which are unique to amorphous silica and have not been found in α-quartz. There have been suggestions that these defects can only be formed at some special precursor sites in a-SiO_2. Again, the definition of the precursor site can differ depending on the method of defect creation, sample treatment and composition.

To summarize, structural disorder should lead to both the distribution of defect parameters and the creation of new defect types. Some of the more general issues pertaining to understanding defects in amorphous materials include the role of local or medium range stress or strain in the surrounding network in defect formation and the definition of a defect model for amorphous material. In a crystal, a defect can be described theoretically in terms of its unique atomic structure and a range of spectroscopic parameters, diffusion mechanisms and barriers and other properties. What would be an equivalent description for an amorphous structure where each site is unique? Can one justify 'average' or 'representative' defect models?

In this paper we briefly review some of the approaches that have been used to address the issues outlined above. We outline the strategies employed to study the distributions of defect properties and focus mainly on the implementation of the embedded cluster method.

We illustrate the results and remaining problems with the example of oxygen vacancy defects in a-SiO_2. The paper is organized as follows. In the next section we outline some of the approaches used to model the structure and properties of defects in amorphous silica. In section 3 we describe the embedded cluster approach. The results for the neutral oxygen vacancies and for the E′ centres are described in sections 4.1 and 4.2 respectively. Finally, discussion and conclusions are in section 5.

2. Approaches to modelling defects in amorphous materials

One way of treating defects in amorphous silica has been to transfer defect models developed for a crystalline phase to the amorphous phase. In particular, the model of the E'_1 centre developed for α-quartz has been considered a natural prototype for the E'_γ centre in a-SiO_2. Following this approach, one needs to search for local regions in an amorphous structure which can accommodate the most stable 'puckered' configuration of the E'_1 centre in quartz. This requires having a 'back oxygen' in the appropriate position to stabilize the puckering Si ion (see figure 1(a)). To find all such sites in the amorphous structure one should express this description in terms of structural parameters characterizing where the back oxygen should be located with respect to the vacancy site. Two similar sets of such 'fingerprints' have been proposed and tested in [6, 39] on the basis of calculated models of E′ centres in a-SiO_2 and in α-quartz.

Understanding the origins of different defect configurations in amorphous materials, such as E′ centres, and predicting their relative concentrations requires correlating the local structural characteristics of oxygen sites in amorphous material—bond lengths, ring size, dihedral angles—with structural models and the properties of defects created at these sites. This is relatively straightforward using theoretical tools: one should build a model of an amorphous structure and then produce defects in a selection of sites and build a distribution of the defect parameters. This approach has been used to study peroxy linkage defects [3] and oxygen diffusion [5], and recently to analyse different kinds of E′ centres in silica [6, 41, 42]. It proved very illuminating, but does not allow one to build good statistics if small periodic cells of amorphous structure are used.

On the experimental front, several studies have analysed the line-shape of EPR signals attributed to E′ centres in different silica samples [29, 30, 44]. In particular, Griscom and Cook [30] have focused on the question of whether the ^{29}Si hyperfine interaction of the E′ centre could be used as a probe of the intermediate range order in silica glass. Employing computer line-shape simulation methods they came up with a hypothesis that most of the E′ centres in the glass samples that they examined existed in backward-projected (or back-projected) dangling bond configurations similar to the model of E'_2 centres discussed by Feigl *et al* [45]. Only a small proportion of E′ centres in these samples would exist in the 'classical' forward-projected dangling bond configuration. Further, Griscom and Cook [30] proposed a set of 'fingerprints' for the back-projected configuration of the E'_γ centre. However, the structure and properties of the back-projected configurations have not been addressed by theoretical modelling.

The fact that concentrations of most intrinsic defects are at the level of 10 ppm makes studying defects unique to amorphous materials particularly difficult. The main problem is that it is unclear whether at equilibrium conditions they exist only at some special precursor sites or at any site in the amorphous structure and how that depends on the previous sample treatment. To find relative defect concentrations, one needs to consider a statistically meaningful number of sites for different defects and for different types of the same defect. The necessity of finding special precursor sites in amorphous structures and considering a large number of sites makes

modelling defects in these materials fundamentally different from that for crystals, where it would be enough to calculate a defect in any of the symmetry equivalent sites. Nevertheless the theoretical models applied in the two cases remain basically the same.

Most of the calculations dealing with defects in amorphous silica have so far been made using either periodic or molecular cluster models. In the first model, the disorder of the amorphous structure is included explicitly, but within a relatively small periodically translated cell (see, for example, [5, 6, 18]). In the second model, a molecular cluster can capture at best the average local structure of the material. A problem pertaining to both models has been that periodic cells and clusters typically include up to 72 atoms which is hardly enough to treat the medium range structural deformation induced by the defect. Another important issue concerns the dependence of the results on the quantum mechanical method (see, for example, [20, 46]). In particular, as has been demonstrated in [39, 47], there can be a dramatic change in the defect electronic structure depending on whether Hartree–Fock or density functional theory (DFT) is used. Besides, neither of the two models can be used to build up significant statistics and to find rare precursor sites. The big advantage of the periodic model is, however, that it can be used to *predict* new defect models, whereas the molecular cluster model has been mainly instrumental in calculating properties of hypothetical defect structures. The major limitations of periodic DFT calculations have been related to predicting too narrow a band gap and the inability to predict optical absorption and luminescence energies of defects.

We are developing a different approach, based on an embedded cluster model of a solid, described in detail below. It is designed to overcome the limitations of both models and to allow one to properly treat the defect-induced distortion of an amorphous network, build up defect statistics and calculate defect spectroscopic properties with good accuracy. We build relatively large samples of amorphous silica using classical molecular dynamics, search for special sites in these structures and then make calculations for defects and their properties at a number of these sites to study the variation of defect properties and determine the relative defect concentrations [42]. As with any other method, the embedded cluster method has its advantages and limitations, which are discussed in the next section.

3. Methods of calculations

The molecular cluster model can be improved by taking into account the interaction of the quantum cluster with the rest of the host lattice, the perturbation of the lattice by the defect and the reciprocal effect of the lattice polarization on the defect itself. This is achieved by constructing an external potential in which the cluster is then embedded and by surrounding the cluster by an infinite polarizable lattice treated classically. Such a potential is called an embedding potential and the model, the embedded cluster model. Accurate representation of the embedding potential is a major challenge, with several approaches existing: see, for example, [46, 48–52].

Most working methods attempt to ‘correct’ the molecular cluster approach mainly by including the Coulomb interaction with the rest of the system. This can be done at three levels of sophistication:

- The electrostatic potential due to the part of the crystal lattice outside the cluster is included in the calculations by: (i) placing point charges of appropriate charge at the lattice sites (see, for example, [53, 54]); (ii) fitting the Madelung potential with several point charges located at specially selected points [55]; (iii) calculating the matrix elements due to the Madelung potential directly and adding these matrix elements to the potential energy matrix [56].

- To further improve the description of the cluster boundary, an interface region between the cluster and the point charges is introduced. Interface atoms can be approximated by effective core pseudopotentials [57, 58] at the cation sites around the cluster or, more accurately, by effective potentials calculated self-consistently specifically for the material under study [54]. The latter approach allows one to reduce the cluster size and the computational load in some cases.
- The defect-induced lattice distortion is accounted for by embedding the cluster in an infinite polarizable lattice of classical ions represented using a shell model [59] or a polarizable ion model [60, 61]. Examples of such schemes can be found in [46, 62–64]. Unlike in the two previous cases, these ions are not kept fixed, but are allowed to adjust their positions to minimize the total energy of the system. This allows one to relax explicitly a large region (several hundred atoms) of the host lattice near the defect. More importantly, embedding into a polarizable lattice can be done in such a way that it also accounts for the effect of the lattice response on the cluster electronic structure. This allows one to achieve self-consistency in the calculation of the defect-induced lattice perturbation and the effect of this perturbation on the defect structure and properties. This effect is similar in many ways to a polaron digging its potential well in a polarizable media.

One of the main advantages of the cluster approach is that it is inherently local in nature and can be easily applied not only to bulk crystals, but also to amorphous materials [39, 87], surfaces [65, 66] and complex interfaces [67]. This method has been used successfully to study defects in ionic crystals [66, 68–70] and its applicability to modelling defects in α-quartz has been demonstrated in recent publications [20, 42, 46]. In the following we briefly describe the preparation and characterization of the a-SiO_2 structures and the details of the embedded cluster method used in this work.

3.1. Preparation and characterization of the amorphous structure

Amorphous silica is a generic name for a wide range of materials of different densities and enthalpies used in the cores of optical fibres and in most silicon-based metal–oxide–semiconductor devices. Theory usually deals with some idealized models of amorphous structure, such as the continuum random network, which can be generated by simulating a melt–quench procedure using classical or QM molecular dynamics. Throughout this work we used an amorphous structure generated using classical molecular dynamics and a 648-atom periodic supercell and NPT ensemble [39]. We followed earlier work by Vollmayr *et al* [71] with several changes summarized below.

We use the DL_POLY code [72] and Buckingham-type inter-atomic potentials developed by van Beest *et al* [73] (BKS). The Buckingham-type potentials contain a dispersion term of $-1/r^6$ (where r is the distance between two atoms) and diverge at small inter-atomic distances. Therefore the BKS potentials were modified to avoid this unphysical behaviour. In particular, we defined a new set of potentials:

$$V(r) = \begin{cases} V_{\mathrm{BKS}}(r) = A\exp(-\alpha r) - C/r^6 & \text{if } r \geqslant r_0 \\ V_{\mathrm{d}}(r) = B\exp(-\beta r) & \text{if } r \leqslant r_0 \end{cases}$$

and derived positive parameters B and β from the conditions

$$V_{\mathrm{BKS}}(r_0) = V_{\mathrm{d}}(r_0)$$
$$V'_{\mathrm{BKS}}(r_0) = V'_{\mathrm{d}}(r_0).$$

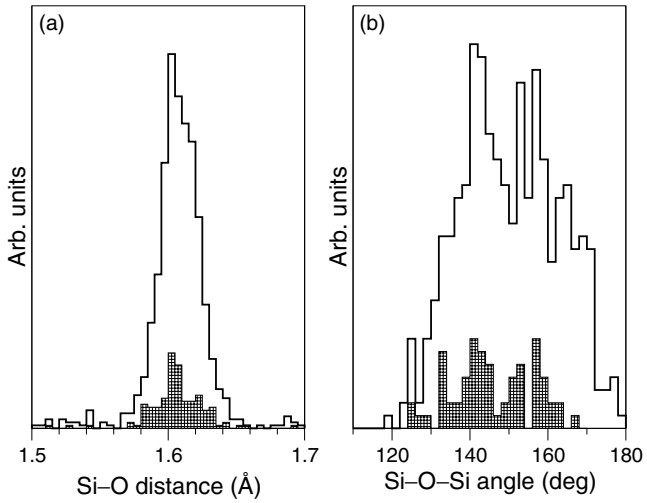

Figure 2. Distributions of: (a) Si–O distances and (b) Si–O–Si angles in MD 648-atom a-SiO_2 structures. The solid parts show the same distributions for the subset of sites chosen for the embedded cluster calculations.

Table 1. Parameters of the classical inter-atomic interaction V_d with a damped van der Waals term.

		Interaction	
Parameters	Units	O–O	Si–O
r_0	Å	1.9	1.18
B	eV	313.9554	505.0553
β	$Å^{-1}$	2.3502	3.5330

The matching point r_0 in the above equations was selected so as to minimize the deviation of $V(r)$ from $V_{BKS}(r)$ in the physically meaningful region of r. The values of parameters B, β and r_0 are given in table 1.

To generate an amorphous structure, we first defined a $2 \times 2 \times 2$ extension of the 24-atom β-cristobalite unit cell and then subjected it to melting, equilibration at high temperature and quenching to low temperature using a molecular dynamics technique and an NPT ensemble. The simulation cell contained 648 atoms and was first heated to 7000 K at a rate of 5×10^{13} K s^{-1} (500 K per 10 ps), then equilibrated at 7000 K for 100 ps and finally quenched to 0 K at a rate of 8×10^{12} K s^{-1} (50 K per 6 ps). The final configuration of the a-SiO_2 structure was further relaxed using static calculations. The results obtained by Vollmayr *et al* [71] suggest that slower quenching would not change the average structural properties of the a-SiO_2 structure.

The resulting a-SiO_2 model proves to be a continuous random network with all the Si ions coordinated with four oxygen ions and all the O ions coordinated with two silicon ions. It has a density of 2.37 g cm^{-3}, which is higher than the average density of 2.20 g cm^{-3} usually attributed to amorphous silica [74]. This reflects the properties of the BKS potentials since the volume of the simulation cell was not fixed during the MD calculations. The distribution of Si–O nearest neighbour distances is given in figure 2(a) together with the distribution of Si–O–Si angles (figure 2(b)). These distributions agree well with those previously reported in

the literature [1]. The structure contains four three-member rings and ten four-member rings but the majority are five- and six-member rings.

3.2. The embedded cluster method

The electronic structure of the a-SiO_2 and that of the defect centres were calculated using an embedded cluster method implemented in the GUESS computer code [65]. Its application to defects in SiO_2 has been thoroughly described in several recent publications [20, 39, 46]. Therefore we will only briefly outline the main features of the method and will focus on the details relevant to studying defects in a-SiO_2.

In broad terms, in the embedded cluster method a system, crystalline or amorphous, with a single point defect is divided into several regions. A spherical region I centred at the 'site of interest' includes:

(i) a quantum mechanically treated cluster (QM cluster),
(ii) an interface region which connects the QM cluster and the rest of the classically treated solid and
(iii) a classical region that surrounds the QM cluster and includes up to several hundred atoms.

Region I is surrounded by a finite region II, also treated atomistically and containing up to several thousand atoms. In the course of calculations, all positions of atoms within region I are fully optimized while atoms in region II remain fixed in the positions corresponding to a perfect crystalline or amorphous structure. Their purpose is to provide a correct electrostatic potential in region I and proper boundary conditions for the atoms at the border of regions I and II. Regions I and II combined together form a finite region which has a radius of several nanometres and is called a *nanocluster*. Finally, to account for the polarization of the solid from the border between regions I and II up to infinity, we introduce region III. It is considered in the approximation of a polarizable continuum and conforms geometrically to the boundary between regions I and II.

The whole approach is similar in spirit to the classical Mott–Littleton method [75]. The total energy of the system includes:

(i) the energy of the QM cluster and the interface atoms in the external electrostatic potentials due to the classical environment;
(ii) the interaction between classical atoms in regions I and II calculated using inter-atomic potentials;
(iii) the short range interaction of both the classical atoms and the interface atoms with the QM cluster atoms calculated using the short range part of the classical inter-atomic potentials; and
(iv) the Mott–Littleton correction for the polarization of region III.

This latter correction is about 0.3 eV in the typical set-up described below and remains constant in all calculations for singly charged vacancies. The expression for the total energy is given in [46].

The classical atoms in regions I and II are represented using the shell model and the rigid atom model, respectively. Their electrostatic interaction with the interface and with the QM cluster atoms is included on the quantum mechanical level, i.e. by calculating the corresponding matrix elements and adding them to the QM potential energy matrix. Total forces on both QM and classical ions are calculated. This allows us to minimize the system total energy simultaneously with respect to the electronic coordinates and the positions of QM

ions and classical ions, and hence to avoid the time-consuming 'self-consistency' procedure used in some previous implementations of this method [76, 77].

The properties of the interface atoms depend on material in question, as described for MgO [65], SiO_2 [46] and Mg_2SiO_4 [69]. For SiO_2, a QM cluster is terminated by the Si^* atoms that form an interface between the QM cluster and the rest of the nanocluster. The Si^* atoms are located at the Si sites of the SiO_2 structure and represent real Si atoms. This is quite different from the case for many molecular cluster schemes where a QM cluster is terminated by artificial so-called pseudo-atoms [31, 78, 79]. The Si^* atoms are chosen so that they are coordinated by one quantum mechanically treated oxygen and three classically treated oxygen ions from the rest of the nanocluster. They perform a dual role: they form a polar bond with the QM oxygen and describe the interaction with the three classical oxygens. This is achieved by representing Si^* as a combination of $\frac{1}{4}$ of a quantum mechanical Si atom and $\frac{3}{4}$ of a classical Si atom. The detailed description of Si^* atoms as applied to α-quartz is given in [20, 46].

This scheme was also used for calculating the distributions of the ground state properties of defects in a-SiO_2 [39, 87]. A more elaborate scheme for the Si^* atoms developed later [40] was used to study the optical absorption of oxygen vacancies. We have checked that the two schemes provide a consistent description of the ground state properties.

The GUESS code [46, 65] plays the role of a 'master' program that calculates the total energy and total forces acting on all centres in region I and performs the geometry optimization of the whole system. Thus the scheme allows us to account consistently for the defect-induced polarization of the host lattice and also the effect of this polarization on the defect itself. The Gaussian-03 package [80] is used for calculations of the quantum mechanical contributions to the total energy and forces.

3.3. Computational set-up for the embedded cluster calculations

Defects formed at different sites of a disordered system can have entirely different properties or structures. To build statistics, one has to consider defects at many sites. Since in the embedded cluster method region I + II should be centred on the defect site, this implies that separate, generally non-equivalent, regions I + II or nanoclusters have to be built for each defect site. Further, the local atomic structure near each site of interest is unique, so QM clusters defined at these sites may have different topologies.

As a consequence, regions I + II centred at different atoms of the a-SiO_2 unit cell will differ in several respects. First, the total numbers of atoms in different nanoclusters are different. Secondly, since region I is defined only by its radius, the total number of atoms in region I will vary from one nanocluster to another. Finally, each nanocluster has a small dipole moment associated with it due to the incomplete cancellation of dipole moments associated with each $Si(\frac{1}{2}O)_4$ 'building block'. This will introduce an additional error in the on-site electrostatic potential inside the nanocluster. As discussed in [39], the effect of these factors is, however, small and can be neglected in the analysis of the results.

Due to poor scaling of Gaussian-03 on parallel computers, calculations for QM clusters greater than about 70 atoms are still quite time-consuming. To explore a large number of sites in the amorphous structure and accumulate good statistics of defect properties we therefore used two groups of QM clusters in these calculations. 'Small' QM clusters were used to explore many different sites and then 'large' QM clusters were used to check the cluster size dependence and to obtain the final values of spectroscopic parameters. 'Small' QM clusters comprise two neighbouring corner-sharing tetrahedra: $Si_2O_7Si_6^*$, where Si^* represent the interface atoms at the border of the QM cluster. The vacancy is then formed at the site of the shared oxygen atom. In the case of the three-member rings, the smallest cluster was either $Si_3O_9Si_6^*$ or $Si_4O_{11}Si_6^*$

depending on the local environment. 'Large' QM clusters are built as extensions of small QM clusters and satisfy two criteria:

(i) *at least* all six Si^* interface atoms of the small QM clusters and their oxygen neighbours are included in the QM cluster; and
(ii) each of the new terminating Si^* atoms should have only one oxygen atom from the QM cluster and three other neighbours from the rest of the nanocluster.

As we discussed earlier [20, 46] defect-induced relaxation is, in general, anisotropic and can result in large displacement of lattice ions even in crystalline SiO_2. In amorphous SiO_2 the situation is complicated by the lattice disorder which makes the distribution of atomic displacements even less predictable. In cases when the defect-induced relaxation results in large displacements and changes of local topology in the vicinity of the interface the QM cluster should be increased to fully include the corresponding region.

We note that the small QM clusters differ in the details of their geometrical structure while the numbers of atoms and the cluster topologies are the same for all cluster sites. On the other hand, the large QM clusters differ in the number of atoms and topology due to disorder of the a-SiO_2 structure.

One of the advantages of this approach is that the electronic structure of QM clusters can be calculated using different techniques. We used both the unrestricted Hartree–Fock (UHF) method and the DFT with B3LYP functional as implemented in the Gaussian-03 package [80]. Standard 6-31G basis sets were used on QM oxygen and silicon atoms and a specially optimized s-type basis function was centred on the interface Si^* atoms.

3.3.1. Describing the interactions between classical ions. A QM cluster, together with the interface Si^* atoms, is surrounded by two spherical regions of atoms treated classically. The inner region, i.e. the classical part of region I, is represented using the classical shell model [59] with modified parameters for inter-atomic interactions taken from [73]. These parameters were modified to account for the polarization of oxygen ions through the shell model and to correctly reproduce the high frequency dielectric constant of α-quartz.

More specifically, we replaced the rigid atom model for oxygen ions by the shell model. The charges of the oxygen core and shell were chosen to be $+0.04e$ and $-1.24e$, respectively. The stiffness of the core–shell spring constant was optimized to reproduce the high frequency dielectric constant of α-quartz and found to be 11 eV $Å^{-2}$.

The interaction between ions in the external region of classical atoms, region II, is described using a rigid ion model and the original BKS potentials [73].

To test the consistency of the rigid and shell model classical potentials, we first compared the geometrical parameters and physical properties of α-quartz calculated using these sets. It is convenient to define the size of the unit cell using the crystallographic notation a, b and c for lengths of primitive vectors (with a being along the x-axis, b being in the xy-plane and c being off the xy-plane). In this case the values of the a and b parameters calculated using the two sets of potentials differ by 0.07%, while c differs by 0.35%. To compare the internal structures, we calculated the difference in fractional coordinates of the atomic cores and found that the largest and average differences were 0.006 and 0.002, respectively. The bulk modulus changed by 4.4% from 40.1 GPa in the rigid model to 42.0 GPa in the shell model. Finally, the static dielectric constant changed by 0.4% for ϵ^0_{11} and ϵ^0_{22} and by 0.7% for ϵ^0_{33}.

To further test the performance of the two sets of potentials we fully relaxed the 648-atom supercell representing an a-SiO_2 structure using both sets and compared the geometrical parameters of the resultant structures. The two sets of potentials produced essentially the same geometrical parameters for the supercell with only a 0.03% difference in the cell volume. The

largest difference in the fractional coordinates of the corresponding atomic cores was 0.0016 which translates into 0.03 Å, while the average difference was 0.017 Å.

Overall, these tests indicate that the original rigid atom BKS potentials and the modified shell model version used in these calculations are compatible with adequate accuracy.

A classical Morse-type inter-atomic potential was also introduced between the interface Si^* atoms and their nearest QM oxygen neighbours. In addition to the pairwise interactions described above, a set of classical three-body potentials of the form $\frac{1}{2}k(\theta-\theta_0)^2$ was introduced at the interface between the QM cluster and the classical region to correct for the distortion of O–Si^*–O and Si^*–O–Si angles (θ) due to imperfect embedding. Since all O–Si–O and Si–O–Si angles in a-SiO_2 are different, separate θ_0 parameters were defined to treat each such angle at the cluster border. The θ_0 parameters were taken as the corresponding angles in the original MD structure. The force constant of 4 eV rad^{-2} was fitted so as to correct the corresponding angles in α-quartz.

3.3.2. Perfect lattice test. To test the accuracy of the embedded cluster method and to compare it with the results of previous studies we carried out the usual routine used in embedded cluster studies, which includes a so-called 'perfect lattice test', i.e. full geometry optimization for the non-defective cluster. In the case of amorphous SiO_2 the reference 'perfect' structure was the 648-atom periodic structure obtained in the MD calculations followed by total energy minimization in the periodic model using the modified BKS potentials with shells on oxygen ions. The largest changes obtained in Si^*–O bond lengths and Si^*–O–Si angles with respect to the ideal structure were 3–5% and 5.5% correspondingly. The deviations obtained for distances and angles in the rest of the system were several times smaller. The effective charges on ions obtained with the natural population analysis (NPA) method [81] were in the range of $2.80 \pm 0.02e$ for silicon ions and $-1.35 \pm 0.01e$ for those oxygen ions which were not neighbours of interface Si^* atoms.

The band gap for α-quartz was calculated as the difference of one-electron energies of the highest occupied and lowest unoccupied molecular orbitals (HOMO and LUMO respectively) using the $Si_8O_{25}Si^*_{18}$ cluster. The calculated value of 8.7 eV can be compared with the experimental value of the α-quartz band gap of 9.65 eV recently obtained using EELS [82] and typical values of absorption band edge in silica glass samples of about 8.96 eV (see, for example, [88]). The distribution of HOMO–LUMO differences calculated for a selection of sites in amorphous SiO_2 has a similar average value and the width of about several tenths of an electronvolt.

Importantly, the topology of the amorphous network in the QM region and at the interface remained the same as that obtained from the original classical MD simulation. Moreover, the displacements of atoms as a result of the embedding procedure are relatively small. This allows us to establish a correlation between the quantum mechanical and classical descriptions of the same lattice sites by comparing the Si–O distances at the centre of each fully relaxed QM cluster with the corresponding distances in the classical calculations. We found that the Si–O distances in the QM calculations are systematically larger than those in the classical calculations by about 0.03 Å. In the following discussion we will correlate the defect properties with the geometrical parameters of the original amorphous structure. For clarity and consistency we will only be using a classical scale for the Si–O distances on the understanding that the QM distances are about 0.03 Å larger.

4. Results of calculations

Our studies focused predominantly on oxygen deficient centres in α-quartz and amorphous silica, which are known to be responsible both for refractive index change in fibre glass through

the Kramers–Kronig and densification mechanisms, and for leakage current and fixed charge formation in CMOS devices. They have been extensively studied experimentally (see, for example, reviews [1, 8, 30]) and include ODC(I) and ODC(II) [8] and various kinds of E′ centres. Still our understanding of their structure and properties remains incomplete.

4.1. Neutral oxygen vacancies

We will first focus on ODC(I), which is diamagnetic and gives rise to an optical absorption band with a maximum at around 7.6 eV in both crystalline quartz and in a-SiO_2. A widely shared opinion attributes this absorption band to neutral oxygen vacancy (NOV) [8, 10, 11], but this assignment has been questioned [83]. A common model of neutral oxygen vacancies in silica has been that of a Si–Si bond formed at the site of missing oxygen atom. Most previous theoretical studies have been performed for α-quartz and support this model [18, 19, 46, 84–86]. However, different methods predict different values for the Si–Si distance, do not take into account the full extent of the defect-induced lattice distortion and contradict each other in terms of optical excitation energies (see [46] for discussion). Below we summarize our results for NOV in α-quartz and in amorphous silica.

4.1.1. Neutral oxygen vacancies in α-quartz. The embedding technique allowed us to perform the first comprehensive analysis of the full extent and character of the lattice relaxation around neutral oxygen vacancies in α-quartz and to show that it induces very strong and anisotropic lattice distortion [46]. The results of these calculations suggest that the rest of the lattice allows the Si atoms to relax without serious inhibition, driven by the Si–Si bond formation. Nevertheless, their strong displacement induces a complicated distortion of the whole region I. The atomic displacements decrease for distant atoms, but the number of these atoms increases rapidly and the resulting effect on defect properties is not negligible.

The absolute values of atomic displacements from the non-defective lattice sites as a function of their distance from the vacant oxygen site are presented in figure 3. One can clearly see that displacements decrease to almost zero (0.01 Å) only at the outer boundary of region I (13.07 Å). They are still about 0.2–0.4 Å at 5 Å from the vacant site and are not negligible even at 10.0 Å from the vacancy. These results significantly alter the model of the neutral oxygen vacancy in SiO_2 as merely a symmetric displacement of the two silicon atoms towards each other due to formation of a chemical bond between them [18, 84].

Our results clearly demonstrate that defect properties strongly depend on the extent of the lattice relaxation accounted for in calculations and on the cluster size and basis set. The vacancy formation energies calculated at the HF level in extended basis sets are broadly in agreement with those found by other *ab initio* methods (see the discussion in [46]). However, the Hartree–Fock calculations of the optical transition energies are less conclusive. They show that the optical absorption energy of the neutral vacancy should be larger than 5 eV. Further time-dependent density functional theory (TDDFT) calculations of the optical absorption, for both ‘small’ and ‘large’ QM clusters, confirmed with greater confidence that this centre could be responsible for the optical absorption with the maximum at 7.6 eV. We also predict a strong backward relaxation in the lowest triplet excited state of the vacancy, and small luminescence energies [46].

4.1.2. Neutral oxygen vacancies in amorphous silica. To study the effect of disorder on NOV in amorphous silica, we used an embedded cluster method to calculate the structure and properties of neutral oxygen vacancies formed randomly at seventy five different sites of the amorphous structure described above. We assumed that neutral oxygen vacancies can be

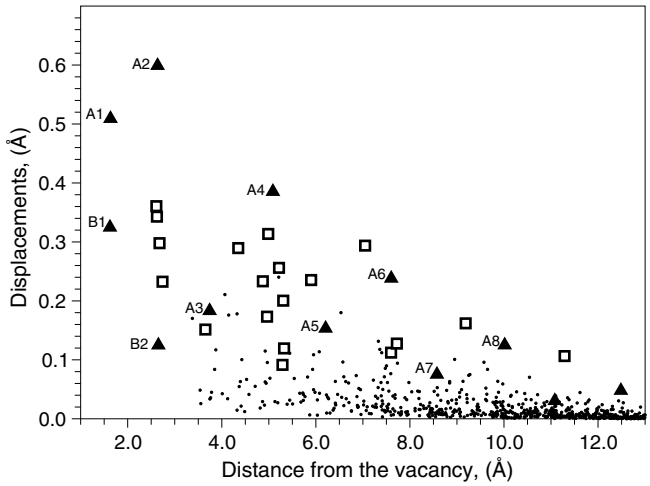

Figure 3. Displacements of lattice atoms induced by the formation of a neutral oxygen vacancy in α-quartz. Dots indicate the atomic displacements induced by the formation of the vacancy. Several atoms that displace in a 'chain-like' motion towards the vacancy as a result of the formation of the Si–Si bond are indicated as solid triangles. Chains Ai ($i = 1, 2, \ldots, 8$) and Bj ($j = 1, 2$) show the displacements of atoms on different sides of the vacancy. Several oxygen atoms that displace considerably following the relaxation of Si–O–Si angles are indicated as squares.

formed at any oxygen site, so their distribution follows the distribution of different sites in the original amorphous structure. The vacancy and its immediate surrounding were treated quantum mechanically using 'small' QM clusters and the 6-31G basis set (see section 3.3). In all cases the selected oxygen site was at the centre of the cluster formed by two adjacent tetrahedra. Each cluster was initially relaxed without the vacancy, as discussed in [39, 42]. Then the neutral vacancy was created by removing the central oxygen atom. The formation energies ($E_{\rm form}$) were calculated with respect to the total energy of the corresponding non-defective QM cluster and free oxygen atom in the triplet state. We also analysed the distribution of defect relaxation energies ($E_{\rm rel}$) defined as the total energy difference between the fully relaxed and unrelaxed systems with the vacancy. This energy is taken as a measure of the defect-induced network distortion. By increasing the QM cluster size for several vacancy configurations we have found no significant dependence of our predictions on the cluster size [87].

The results demonstrate a wide distribution of local defect configurations with Si–Si bonds ranging from 2.3 to 2.7 Å. In all cases we find that the removal of an oxygen atom is accompanied by Si–Si bond formation. The distance between the two Si ions becomes much shorter than the original distance and as Si ions move closer to each other they pull the network ions with them. However, the bond length and details of the lattice relaxation in the vicinity of the defect depend on the structure of the local and medium range environments of the original site. These properties can be characterized in terms of distributions of structural and energetic parameters. For example, the distribution obtained for oxygen vacancy formation energies is shown in figure 4(a). It has a full width at half-maximum (FWHM) of about 1.8 eV with the maximum between 4.2 and 4.4 eV. The latter should be compared with the formation energy of 4.5 eV [46] for an oxygen vacancy in α-quartz calculated using a QM cluster of the same size.

Further analysis of the medium and long range relaxation of the amorphous network induced by the formation of neutral vacancies demonstrates that, as in α-quartz (see [46]), this

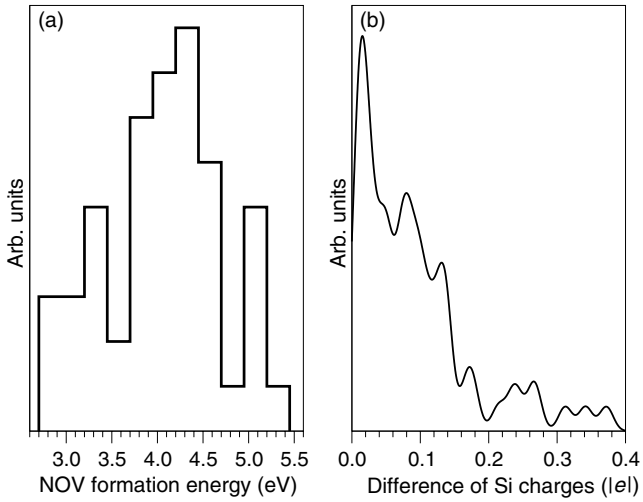

Figure 4. Properties of neutral oxygen vacancies in a-SiO_2. (The statistics are taken over 75 sites.) (a) Distribution of formation energies; (b) distribution of differences in atomic charges of Si atoms neighbouring the vacancies.

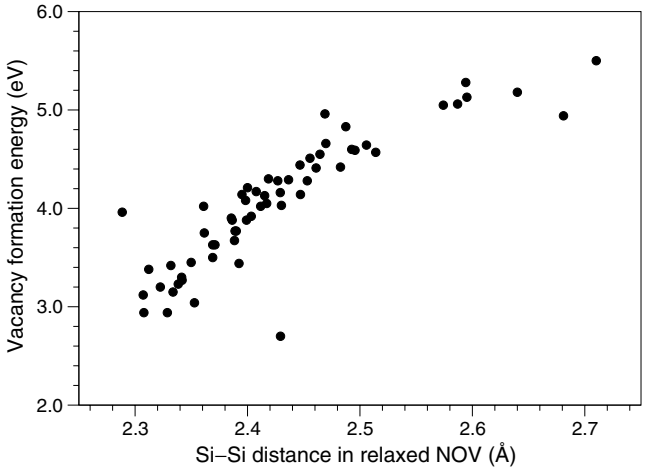

Figure 5. Correlation between the Si–Si distances in relaxed neutral oxygen vacancies and the formation energies of these vacancies.

relaxation is very long ranged. However, the character of this relaxation can be even more complex. For example, in some cases the two Si atoms near the vacancy displace less than their neighbouring oxygen atoms. This is accompanied by a large distortion of the Si–O–Si angles associated with the oxygen atoms. Since the tetrahedral O–Si–O angles do not change much (about 2°) the oxygen plane shifts with respect to the Si atom closer to the vacancy. Overall, the network relaxation shows compaction near the vacancy site. We found a strong correlation between the vacancy formation energies and the Si–Si distance in relaxed vacancies (figure 5), shorter distances corresponding to smaller formation energy. This suggests that at thermodynamic equilibrium, which can be achieved e.g. in annealed thermal oxides on Si and some glasses, vacancies will preferentially have short Si–Si bond lengths.

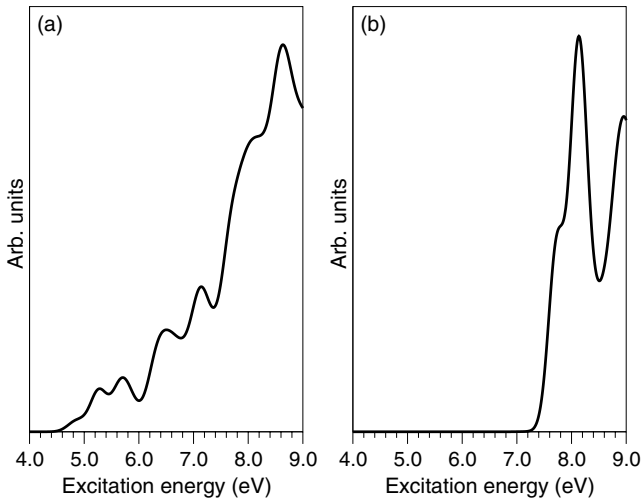

Figure 6. Optical absorption spectrum calculated for 23 neutral vacancy configurations at different lattice sites. (a) The 'as calculated' absorption spectrum. (b) The absorption spectrum after it was weighted with the Boltzmann factor and corresponding vacancy formation energy.

We have also found a strong correlation between the NOV optical absorption energies and the Si–Si bond lengths with shorter bond lengths corresponding to higher optical transition energies. Assuming that low formation energy vacancies dominate at thermal equilibrium, we compared two optical absorption spectra calculated using TDDFT. One spectrum, shown in figure 6(a), was obtained by summing up the individual spectra obtained for each of the 23 sites included in a set of the 20 lowest formation energy sites and 3 sites with medium and high formation energies (see [87] for details). The envelope curve is produced by broadening each transition with excitation energy E_i by a Gaussian-type function $f_i(E) = \exp(-(E - E_i)^2/2\sigma^2)$ with the σ parameter equal to 0.15 eV. The spectrum obtained is shown in figure 6(a); it shows a maximum at approximately 8.5 eV and a prominent tail that reaches to 5 eV in the red part of the spectrum.

The low energy part of the spectrum is mainly determined by the transition between the bonding σ and anti-bonding σ^* states of the NOV. Both states are located in the band gap and contribute to optical transitions up to 7.8 eV. Our analysis suggests that the splitting between the one-electron energies of σ and σ^* states is smaller for the vacancies with longer Si–Si bonds. This is confirmed by an anti-correlation found between the Si–Si bond lengths and the energies of the bonding (σ)–anti-bonding (σ^*) transitions [87]. At the same time, longer Si–Si bonds correspond, statistically, to vacancies with larger formation energies (see figure 5). Consequently, we can correlate the low energy tail of the optical absorption with the vacancies that have larger formation energies.

At higher energies, the optical absorption is dominated by transitions between the σ and π states of the vacancies and transitions between the valence band states and σ^* and π states of the vacancies. The oscillator strength of these transitions is typically several times lower than that for the main transitions from bonding σ to anti-bonding σ^*. A further contribution to the absorption spectrum comes from band-to-band transitions. The transitions of this type included in the first 25 excited states contribute to the peak at approximately 8.5 eV (see figure 6(a)).

To take into account only the most populated vacancy configurations at thermal equilibrium, the optical absorption spectrum was then weighted with the Boltzmann factor

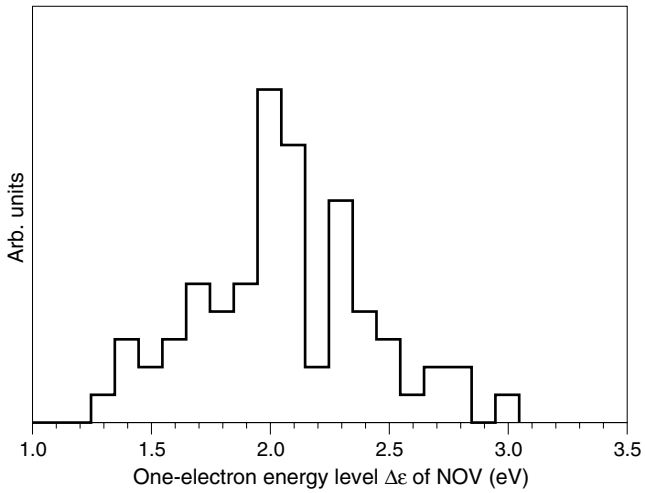

Figure 7. Distribution of the one-electron energy levels of NOVs with respect to the top of the valence band.

$\exp(-E_{\text{form}}/kT)$, where E_{form} is the vacancy formation energy calculated using the B3LYP functional, k is the Boltzmann constant and T is temperature. The spectrum shown in figure 6(b) was calculated for $T = 300$ K. After the adjustment for the vacancy formation energies, the shape of the absorption spectrum has changed considerably: the tail between 5 and 7 eV has disappeared and the maximum at 8.5 eV has shifted to 8.1 eV. Due to their large formation energies the long bonded Si–Si configurations included in the selection of 23 NOV sites do not contribute to the weighted optical absorption spectrum at room temperature. Therefore the tail reflects the presence of the vacancies with Si–Si bond lengths exceeding those found for vacancies with the lowest formation energy, i.e. around 2.3 Å. Thus, the optical absorption in the energy range of 6–7 eV reported, for example, in [88] could reflect the distribution of the Si–Si distances in a particular sample.

The formation of a neutral oxygen vacancy induces a doubly occupied energy level in the silica band gap. The position of this level with respect to the top of the valence band can be characterized using a parameter $\Delta\epsilon$ defined as the difference between one-electron energies of the highest occupied state of the valence band (HOMO) and the vacancy state. The distribution of $\Delta\epsilon$ calculated for NOVs at 75 sites is shown in figure 7. The HOMO only approximately represents the position of the top of the valence band in the material as it is affected by the particular position of the NOV in the amorphous network and by the degree of the NOV-induced lattice distortion. Nevertheless, the broad distribution seen in figure 7 clearly demonstrates the extent of inhomogeneous broadening of defect levels in amorphous silica and could be relevant to the possible role of NOV in MOS devices [1].

4.2. Models and properties of E′ centres in silica

4.2.1. E_4' and E_1' centres in α-quartz. Prior to embarking on an extensive study of oxygen vacancies in a-SiO_2, we investigated the structure and EPR parameter of E_4' and E_1' centres in α-quartz [20]. The EPR properties of these defects have been studied experimentally and they are perhaps the best understood defects in α-quartz. The results are in good agreement with the experimental data and the results of periodic DFT calculations. However, our calculations give generally better agreement of the calculated hyperfine (hf) and superhyperfine (shf)

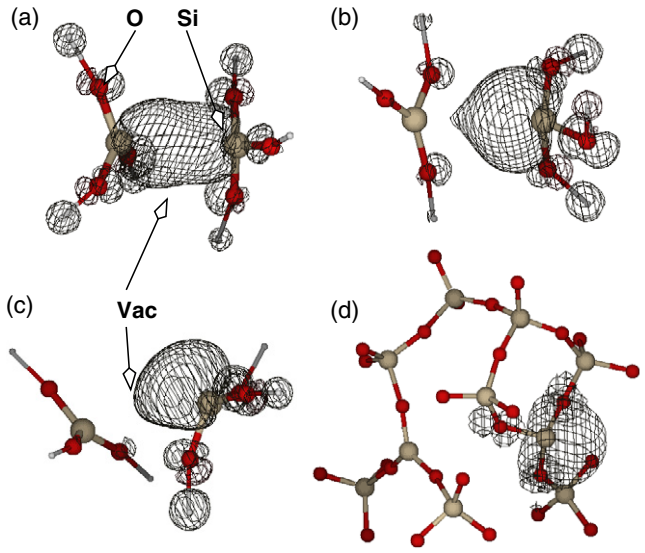

Figure 8. Spin density distributions in different kinds of E′ centres: (a) dimer configuration, (b) intermediate configuration, (c) dangling bond (DB) configuration, (d) back-projected configuration. (a)–(c) were calculated using 'small' QM clusters, and (d) was calculated using a 'large' cluster. **Vac** indicates the vacancy site.

constants with the experimental data than most previous studies. Moreover, we have been able to calculate the g-tensor for E_1' centre in α-quartz and found that the principal values are 2.001 88, 2.000 43, and 2.000 27, which is again in good agreement with experimental results of Silsbee [13] (2.001 76, 2.000 49 and 2.000 29) and Jani *et al* [14] (2.001 79, 2.000 53 and 2.000 30). We have also elucidated the nature of the optical absorption of E_1' centres in α-quartz discussed earlier by Pacchioni *et al* [78] on the basis of their molecular cluster calculations. Our embedded cluster calculations of the optical absorption of E_1' predict two transitions with different energies. The strongest excitation at about 6.3 eV involves electron transitions from the occupied defect-induced resonant states in the valence band to the unoccupied defect state localized in the vacancy and the unoccupied defect-induced states in the conduction band. The electron transfer transition to the puckered silicon ion is at 4.4 eV and has a much lower probability.

4.2.2. Models of E′ centres in amorphous silica. Some of the positively charged vacancies, such as E_γ' centres, in thermal oxide and in silica glass are formed by hole trapping by neutral vacancies. Using the NOV calculations we created a corresponding distribution of E′ centres in amorphous silica formed as a result of ionization or hole trapping by pre-existing neutral oxygen vacancies. This approach allows us to find different structural kinds of positively charged vacancies. We demonstrate that hole trapping by these vacancies will lead to formation of broadly two kinds of E′ centres—dangling bond (DB) and dimer-type centres (see figure 8). We found several configurations of dangling bond centres, which include the classical puckered configuration, as well as unpuckered and back-projected ones. Some of the dimer configurations could transform into the dangling bond configurations. The conditions for formation of these different defect structures are discussed in [39]. We verified our findings by comparing the calculated hyperfine and superhyperfine EPR parameters and optical absorption energies with the experimental data. We studied the dependence of the results on the method

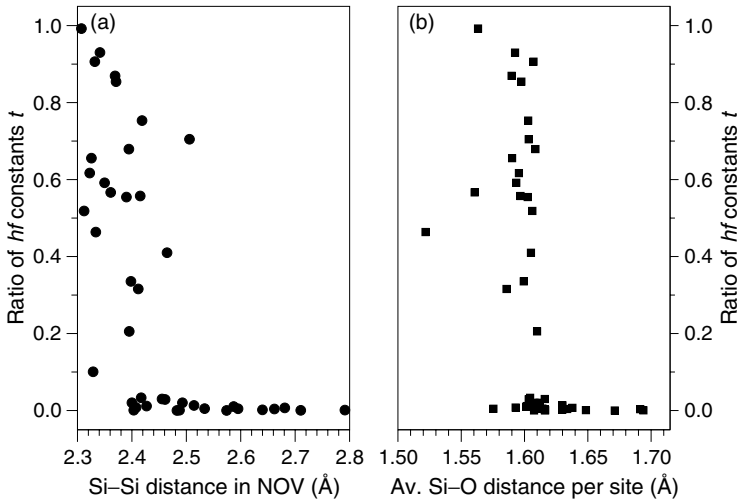

Figure 9. (a) Correlation of the ratio of the hyperfine constants on the neighbouring Si atoms in the E′ centre configuration t with the Si–Si distance in the parent neutral vacancy. (b) Correlation between the same ratio t of the Si hyperfine constants and the average Si–O distance at the corresponding oxygen site in the original amorphous structure.

of calculation and demonstrated that the character of localization of an unpaired electron in positively charged oxygen vacancies depends on the amount of exact exchange contribution in the density functional employed.

The distribution of the spin density between the two Si atoms near the vacancy for the main kinds of positively charged vacancies in our amorphous structure is shown in figure 8.

To understand better the origins of these structural kinds of E′ centres we attempted to link them with the local atomic structure of their precursors—neutral vacancies. For that purpose we introduced a parameter t—the ratio of the hyperfine constants on the two Si ions a_{Si_1} and a_{Si_2} neighbouring the vacancy, and correlated it with the structural parameters of neutral vacancies. The parameter t is defined as $t = a_{\mathrm{Si}_1}/a_{\mathrm{Si}_2}$, where $a_{\mathrm{Si}_1} < a_{\mathrm{Si}_2}$. The dimer-type configurations are characterized by similar hyperfine constants on both Si ions resulting in t being close to unity. In the dangling bond configuration, the spin density is almost completely localized on one Si ion and t is close to zero.

As one can see in figure 8, the local atomic structure of the lattice plays an important role in determining the type of the E′ centre formed. In particular, the difference in relative orientation of the tetrahedral units surrounding the vacancy between the dimer and the unpuckered E′ centre, shown in figures 8(a) and (c) respectively, is clearly visible. To characterize this feature even further, in figure 9(a) we show the correlation between the Si–Si distance in the neutral vacancy configuration and the ratio t for the corresponding positively charged vacancies. One can see that, if the Si–Si distance in the precursor neutral vacancy is less than 2.4 Å, the ionized state shows the ratio t to be predominantly larger than 0.5, which corresponds to the dimer configuration and some intermediate configurations. For Si–Si distances between 2.4 and 2.5 Å one obtains the intermediate and dangling bond configurations. Longer distances always result in dangling bond configurations.

One can also distinguish three kinds of displacements of Si ions following relaxation from a neutral vacancy into an ionized configuration. The formation of dimer-type centres is characterized by relatively small displacements of atoms from their positions in the

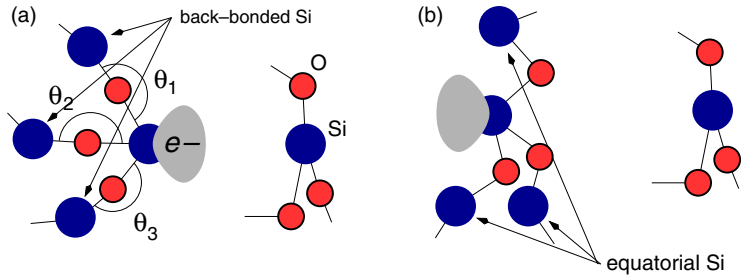

Figure 10. A criterion used to search for back-projected configurations of E′ centres in a-SiO_2. (a) Select sites with angles θ_1, θ_2 and θ_3 are close to 180° simultaneously. (b) Atomic structure of a back-projected configuration of an E′ centre.

precursor neutral vacancy, rather similar to those in a dimer-type E′ centre in α-quartz (the Si displacements around 0.3 Å, maximum). In this case the two Si ions do not fall far apart, so the Si–Si bond could still be preserved. The stronger relaxation from a neutral vacancy (around 0.5 Å) is characteristic of intermediate-type centres, and in most dangling bond centres the two Si ions find themselves much further apart with a large displacement (maximum of 1.0 Å) from the initial neutral vacancy configuration. This relaxation is determined by both the initial short and medium range structures and is accompanied by the reorientation of surrounding tetrahedra.

If neutral vacancies are formed with equal probability at any oxygen site in the original amorphous structure, what should the relative concentrations of the different kinds of configurations be? In [42] we suggested that the average Si–O distance D for a given oxygen site defined as $D = (d_1 + d_2)/2$, where d_1 and d_2 are distances between the oxygen atom and its Si neighbours in the initial amorphous network (see also figure 9(b)), can serve as a useful parameter determining which type of positively charged oxygen vacancy could be formed at a particular oxygen site. This parameter takes into account that in the tetrahedral structure of silica the oxygen vacancy site is not directly on the Si–Si line. The plot of the ratio of hyperfine constants t as a function of the parameter D is presented in figure 9(b). It clearly demonstrates that for $D < 1.62$ Å all defects are of the dimer or intermediate type, whereas for $D > 1.62$ Å only defects of the dangling bond type are formed. One can therefore use D for predicting relative concentrations of different defect types [42]. However, as discussed in [39], the result depends on the calculation method: calculations using density functional theory and density functionals with small exact exchange contributions tend to favour dimer configurations over dangling bonds.

4.3. Properties of E′ centres in amorphous silica

How do we relate these findings to the properties of E′ centres in amorphous silica identified experimentally? It has long been thought that the E'_γ centre in a puckered configuration predicted in [15] is the most common type of E′ centre in amorphous silica. However, the results of theoretical calculations suggest that the number of sites which could accommodate puckered E'_γ centres in a continuous random network amorphous silica structure is of the order of 10% of all oxygen sites [6, 39]. If one assumes that all oxygen sites are equally amenable to formation of E′ centres, this may suggest that the unpuckered configuration (see figures 8 and 11(c)) could be much more common because it does not require the special precursor sites for its formation. However, this assumption is not justified for most formation mechanisms for E′ centres except hole trapping by neutral oxygen vacancies. Indeed, the exciton decomposition mechanism [89] or the one involving cleavage of Si–H bonds (see, for

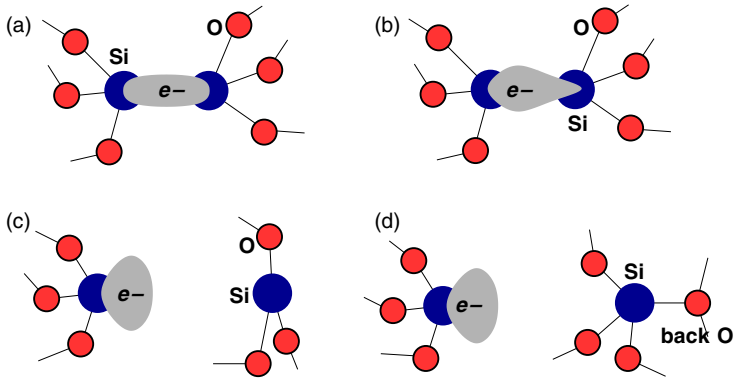

Figure 11. Most probable kinds of E′ centres suggested on the basis of medium range order in a-SiO_2. (a) Dimer; (b) intermediate (distorted dimer); (c) unpuckered dangling bond (DB) type: the unpaired electron is fully localized on a single Si atom, while the other Si atom moves to the plane of the neighbouring oxygens; (d) puckered: similar to (c) but the second Si atom is tetrahedrally coordinated due to the presence of a back oxygen.

example, [43]) may lead to different results. The results of calculations suggest, however, that it might be difficult to distinguish between puckered and unpuckered configurations on the basis of hyperfine interactions alone as they are very similar for the two kinds of centres [39].

There is still also controversy regarding the structure of the E'_δ centre in amorphous silica and whether it is a stable or a metastable defect. In particular, the experimental results of Griscom and Friebele [25] and Zhang and Leisure [26] suggest that this is a rare defect with quite an exotic structure that may involve four Cl atoms in the SiO_4 vacancy. On the other hand, if the silicon dimer model proposed by the theory [27] is correct, this could in fact be a very common defect with one of the simplest structures in silica. The theoretical results obtained recently by Lu *et al* [6] suggested that the vast majority of positively charged oxygen vacancies are not bi-stable as in α-quartz, but the silicon dimer configuration is in fact the only stable defect in 80% of the oxygen sites.

The results of our calculations [40] also support the dimer model of the E'_δ centre [27]. The highest occupied orbital for a typical dimer centre is shown in figure 8(a). The calculated hf splittings due to the interaction of the unpaired spin with two Si ions of the dimer are 10.5 and 10.0 mT. These are close to those measured experimentally for the E'_δ centre [25, 26]. These hf constants are not equal due to the lattice disorder, which affects the local structure of this particular site. The width of the distribution of hyperfine parameters due to disorder, estimated from several configurations found in our calculations, is 5.0 mT. The main reason for these relatively small values of the hf splitting is seen in figure 8(a)—the unpaired electron density in the dimer configuration is delocalized to a large extent *between* the two Si ions reducing the s orbital contribution to the Si nuclei. The components of the g-tensor given in table 2 are much more isotropic than those for the DB configuration and are close to those attributed to the E'_δ centre [25].

We used TDDFT to calculate the optical transition energies for this centre. The main optical transition is due to $\sigma \rightarrow \sigma^*$ excitation; it has an energy of 6.3 eV and an oscillator strength of $f = 0.35$. The $\sigma \rightarrow \pi$ transition has an energy of 7.3 eV and an oscillator strength of $f = 0.03$. The higher energy transition at 7.9 eV, which has a mixed character with contributions from $\sigma \rightarrow \pi^*$ excitations and from VB $\rightarrow \sigma^*$ excitations, has a higher oscillator strength of 0.12. These transitions overlap with the broad spectrum attributed to the E'_γ centre and NOV in irradiated glass samples [9].

Table 2. The theoretical and experimental values of the g-tensor components and optical absorption energies for the E′ centre configurations discussed in this paper (see also figure 8).

Structural configurations	g-tensor		Optical excitation energy (eV)	
	Theory	Experiment [25]	Theory	Experiment [88]
E'_δ (dimer)	2.0018	2.0018		
	2.0034	2.0021	6.33	—
	2.0043	2.0021		
E'_γ (DB)	2.0018	2.0018		
	2.0008	2.0003	4.0 and 5.8	5.8
	2.0007	2.0006		
Back-projected E′	2.0018			
	2.0010	—	5.5–5.6	—
	2.0008			

Another E′ centre type, not previously predicted theoretically, is the so-called back-projected configuration suggested by Griscom and Cook [30]. They pointed out that analysis of superhyperfine constants of E′ centres may provide some insight into the medium range glass structure around them and suggested geometric criteria for formation of the back-projected configuration based on dihedral and Si–O–Si angles. In simple terms, these criteria imply that, if all three Si–O–Si angles (θ_1, θ_2, θ_3 in figure 10(a)) with the so-called back bonded silicon ions in the non-defective lattice or in the neutral vacancy configuration are close to 180°, then the E′ centre formed at this site is likely to become back-projected after relaxation, as shown in figure 10(b). In other words, it will not have any back bonds at all. Based on this analysis they estimated that 35%–80% of all E′ centres in their sample have this property. They are characterized by hyperfine constants of about 41.9 mT and superhyperfine constants of 0.3 mT.

In [39] we discussed the structure of the back-projected configuration of the E′ centre and the conditions for its formation in amorphous silica. Essentially such a configuration can be formed if a silicon ion that hosts the unpaired electron, shown as Si_1 in figure 8(d), puckers through the plane of three nearest neighbour oxygen ions. The conditions for formation of this configuration were first formulated in [30]. Our results demonstrate that stable back-projected configurations can be formed if the inverted dangling bond faces the ample free space provided by the surrounding ring structure. However, the barrier for the formation of this configuration is about 1.5 eV and the barrier for the reverse process is about 1.0 eV. The typical values of hyperfine and superhyperfine constants are 43.1 and 0.26 mT, 0.23 and 0.29 mT, respectively [39] and the calculated components of the g-tensor of this centre are shown in table 2.

The optical absorption spectrum is formed by a group of transitions with energies close to 5.6 eV and relatively small oscillator strengths of about 0.012–0.025. Most of these transitions can be described as excitations from the defect-induced occupied states in the valence band into the unoccupied p states associated with the back-projected Si ion. The nature and energies of these transitions are again close to those attributed to the E'_γ centre in irradiated silica samples [9].

5. Discussion and conclusions

A consistent picture emerges from our work for the possible configurations of neutral and positively charged oxygen vacancies in amorphous silica. Neutral vacancies are characterized by a wide distribution of formation energies and structural parameters. Positively charged

Table 3. Hyperfine constants (mT) for E′ centres formed at different sites. Si_n ($n = 1, 2$) and Si_{ni} ($i = 1, 2, 3$) are the nearest and the second-nearest neighbours of the oxygen vacancy respectively.

			Si_{1i} shf				Si_{2i} shf		
Type of E′ centre	Figure	Si_1 hf	Si_{11}	Si_{12}	Si_{13}	Si_2 hf	Si_{21}	Si_{22}	Si_{23}
Dimer-like	11(a)	10.9	0.08	0.17	0.04	12.1	0.05	0.35	0.35
Unpuckered	11(c)	44.3	1.33	0.50	0.07	0.0	0.03	0.00	0.00
Puckered with O_B	11(d)	43.0	1.13	0.80	0.20	0.0	0.00	0.00	0.00
Back-projected	8(d)	43.1	0.26	0.23	0.29	0.0	0.00	0.00	0.00
Back-projected with O_B	—	48.9	0.45	0.02	0.25	0.0	0.00	0.00	0.00
E'_δ: experimental [25]		10.0							
E'_γ: experimental [90]		41.9	1.3	0.3					
E'_γ: experimental [91]		41.9	0.8	0.3					

vacancies form two major structural types: dimer and dangling bond centres. We predict that most dangling bond centres are unpuckered, as shown in figure 11(c), and demonstrate that most configurations of the dangling bond centres have similar hyperfine EPR parameters. Our results confirm the possibility of existence of the back-projected E'_γ centre configuration and suggest that such centres can be stable in a larger number of sites than has been proposed from experiment [30]. We also suggest that the puckered configuration is not the dominant configuration of the E'_γ centre in amorphous silica.

Our approach differs from those used in similar previous studies in several respects. Many molecular cluster calculations (see, for example, [27, 32, 78]) are not based on any particular a-SiO_2 model and so can capture only those defect properties which are determined by the most stable *local* properties of the material. Our calculations explore a well-established model of an amorphous structure and allow us to treat consistently the local, medium range and long range environment of each defect site. In addition we can build a statistical distribution of defect properties and relate these properties to the structure of the amorphous network. Besides this, the embedded cluster model allows one to properly account for variations of the electrostatic potential in the amorphous network and for its polarization by the charged defect.

Our calculations demonstrate the strong long range lattice relaxation induced by most of the oxygen vacancies. This effect cannot be fully accounted for by using molecular clusters and periodic calculations. This might be one of the reasons that earlier theoretical calculations could not predict e.g. the unpuckered DB-type defect. Other configurations may also exist although we did not find them. Extending the behaviour of the Si atoms we predicted that there could be, for example, double puckering when both the Si atoms have back oxygen atoms (O_B) and even more complex configurations (see [39]).

It is interesting to note that the unpuckered DB configuration basically corresponds to that suggested by Yip and Fowler [17] as a model of the E'_1 centre on the basis of small cluster calculations some 30 years ago. But it has never actually been *predicted* in theoretical calculations of amorphous structures. Moreover, it has been suggested in [31] that the ionization of a neutral vacancy would always produce a dimer configuration (with the exception of vacancies formed on the edge of edge-sharing tetrahedra). The typical hf and shf constants for these configurations are given in table 3. The hf constants of the DB-type defects are similar to those assigned to the E'_γ centre in a-SiO_2 in experimental [10, 30] and other theoretical [18, 19, 32, 33] studies. However, unlike in the case of the E'_γ centre, this configuration does not require any back oxygen (O_B). Our calculations suggest that this could be the most abundant type of E′ centre obtained

by ionizing pre-existing neutral vacancies in amorphous silica. Other types, such as the puckered and back-projected configurations, require more specific conditions for their stabilization. We note, however, that our calculations suggest that the conditions for existence of stable back-projected E′ centres are much less strict than originally suggested in [30]. In fact, only a sufficiently large void space is required to stabilize E′ centres in the back-projected configuration.

The hf constants given in table 3 belong to different kinds of DB-type E′ centres, distinguished by their shf constants. The hf constants of these centres are similar and fall within the full width at half-maxima (FWHM) of E'_γ centres in a-SiO_2. The shf constants for the unpuckered E′ centres and classically puckered E′ centres are similar as both have a weak shf constant of about 1.1 mT. For back-projected E′ centres, the Si atom possessing the unpaired electron points away from the vacancy and there is no 'weak' shf interaction, but only 'very weak' shf interaction, as observed experimentally [29, 30].

We have calculated the hyperfine parameters, *g*-tensors and optical excitation energies for the dimer and back-projected configurations of the E′ centre in amorphous silica. The EPR parameters are in good agreement with the experimental values attributed to the E'_δ centre and the back-projected configuration of the E'_γ centre in silica glass. The optical transition energies are calculated for the first time and could be used for further experimental identification of these centres. We should note that the optical spectrum of these centres will be broadened due to the varying local and medium range environments of different sites in an amorphous network. The predicted energies at around 6.3 and 5.6 eV overlap strongly with the broad spectrum attributed to the E'_γ centre. This implies that confident identification of these configurations may require analysis of both optical absorption and photoluminescence spectra.

Our results support the dimer model of the E'_δ centre and for the first time provide a full range of spectroscopic parameters for the back-projected configuration of the E′ centre in amorphous silica. However, they do not exclude the existence of the other models of the E'_δ centre in specific types of silica glass described in section 4.2. Since the optical absorption of other models of E'_δ is expected to differ considerably from the one considered here, our results may help to identify particular kinds of E'_δ centres. Thus, the embedded cluster method combined with classical MD for generating the amorphous structure can be used for predictive modelling of defect properties in amorphous silica.

We note that our results predict that dimers are the minority species with respect to other positively charged oxygen vacancies rather than the majority species predicted in [41, 6]. As discussed in [39], this discrepancy between the two studies results from the different methods used: plane wave DFT tends to delocalize weakly bound electronic states, which led to the disproportionally large number of dimers obtained in [6, 41]. On the other hand, the Hartree–Fock method used in [39], tends to favour localized solutions. The very fact that we obtained several dimer configurations in a strongly disordered structure using this method testifies in favour of their existence. However, we should note that most of these configurations are distorted and for some types of local environment for these vacancies we find that there exists the alternative more stable dangling bond type of configuration.

The continuum random network provides a smooth distribution of structural parameters, such as bond lengths, angles and rings. In this case, the challenge concerns correlating defect properties with local and medium range properties of the amorphous network. Exploring different sites and building up statistics is important because this could allow one to find reliable correlations between the network structure and defect properties and hence engineer the amorphous structure to achieve desirable concentrations of particular defects. In particular, there have been suggestions that the low energy tail in the optical absorption of amorphous silica could be determined by three-membered rings in the amorphous network [92]. Therefore reducing the number of these rings could lead to an increase in the transparency gap of a glass.

Configurations discussed above were obtained by single ionization of a precursor neutral vacancy. In reality, though, precursor sites for defect creation depend on the mechanism of defect formation. On one hand, there is no clear reason for believing that neutral vacancies are distributed homogeneously in amorphous structure, as assumed in this paper. On the other hand, in irradiated samples E′ centres are formed due to exciton decomposition into a pair of Frenkel defects [93]. In this case, the structure and the spatial distribution of defects depend on where stable defects can be formed in a particular amorphous structure. In most cases silica samples are irradiated by large doses of ionizing radiation or by powerful laser pulses. In these cases, multiple secondary processes involving sequential electron trapping and ionization of the same defect can be important. These processes can tip the balance of different configurations, increasing the concentration of e.g. back-projected or even more complex configurations. Therefore the real value of such correlations often depends on the mechanisms of defect creation.

Our results, like those of previous workers, clearly highlight issues which should be addressed in further studies. The key issue remains an accurate prediction of relative concentrations of different defect types. It is hampered by several factors.

First, it is based on an assumed mechanism of formation of positively charged vacancies via hole trapping by neutral vacancies. One should also take into account the distribution of neutral vacancy formation energies and radiation mechanisms via exciton decomposition into defect pairs, which may both lead to different (and inhomogeneous) distributions of defects. Careful studies of exciton configurations and their possible decay channels are required. Analysis of the correlation between the local atomic structure, exciton properties and the mechanisms of defect pair formation will help to address the question of the relative concentration of defects.

Second, the defect types (for example dimer versus dangling bond) formed in particular network sites are sensitive to the quantum mechanical method used in calculations [39]. Therefore, the structural criteria that relate the defect type to the structural properties of individual sites in the amorphous network ('fingerprints') should be based on reliable methods to be useful in predicting possible defect concentrations. Development of such methods represents a major challenge since they have to provide accurate electronic structures of both ground and excited states and yet remain computationally efficient. In addition, the models used in the calculations are expected to allow for defect-induced lattice relaxation and interaction between the defects including defect recombination, aggregation as well as charge transfer between them. Our results suggest that these objectives can be achieved via further development of the embedded cluster approach.

Acknowledgments

The authors would like to thank A H Edwards, A M Stoneham, K Tanimura, D L Griscom, S Agnello, V Mashkov, I V Abarenkov and K Mallik for many useful discussions. We are grateful to C Bird for his comments on the manuscript. The work was supported by EPSRC, Japan Science and Technology Corporation, US Airforce through EOARD, and by the Grant-in-Aid No 16GS0205 for Creative Research from the Japan Ministry of Education, Culture, Sports, Science and Technology. The computer time on the HPCx facility was awarded to the Materials Chemistry consortium under EPSRC grant GR/S13422/01 'Materials Chemistry using Tera-Scale Computing'.

References

[1] Pacchioni G, Skuja L and Griscom D L (ed) 2000 *Defects in SiO_2 and Related Dielectrics: Science and Technology* (*NATO Science Series, Series II: Mathematical and Physical Chemistry*) (Dordrecht: Kluwer)

[2] Devine R A B, Duraud J-P and Dooryhée E (ed) 2000 *Structure and Imperfections in Amorphous and Crystalline Silicon Dioxide* (New York: Wiley)
[3] Szymanski M A, Shluger A L and Stoneham A M 2001 *Phys. Rev.* B **63** 224207
[4] Donadio D, Bernasconi M and Boero M 2001 *Phys. Rev. Lett.* **87** 195504
[5] Bongiorno A and Pasquarello A 2002 *Phys. Rev. Lett.* **88** 125901
[6] Lu Z-Y, Nicklaw C J, Fleetwood D M, Schrimpf R D and Pantelides S T 2002 *Phys. Rev. Lett.* **89** 285505
[7] Wright A C 2000 *Defects in SiO_2 and Related Dielectrics: Science and Technology* (*NATO Science Series, Series II: Mathematical and Physical Chemistry*) ed G Pacchioni, L Skuja and D L Griscom (Dordrecht: Kluwer) pp 1–35
[8] Skuja L 1998 *J. Non-Cryst. Solids* **239** 16–48
[9] Skuja L 2000 *Defects in SiO_2 and Related Dielectrics: Science and Technology* (*NATO Science Series, Series II: Mathematical and Physical Chemistry*) ed G Pacchioni, L Skuja and D L Griscom (Dordrecht: Kluwer) pp 73–116
[10] Guzzi M, Martini M, Palear A, Pio F, Vedda A and Azzoni C B 1992 *J. Phys.: Condens. Matter* **4** 8635–48
[11] Schurman M K and Tomozawa M 1996 *J. Non-Cryst. Solids* **202** 93–106
[12] Weeks R A and Nelson C M 1960 *J. Am. Ceram. Soc.* **43** 399–404
[13] Silsbee R H 1961 *J. Appl. Phys.* **32** 1459–62
[14] Jani M G, Bossoli R B and Halliburton L E 1983 *Phys. Rev.* B **27** 2285–93
[15] Rudra J K and Fowler W B 1987 *Phys. Rev.* B **35** 8223–30
[16] Allan D C and Teter M P 1990 *J. Am. Ceram. Soc.* **73** 3247–50
[17] Yip K L and Fowler W B 1974 *Phys. Rev.* B **11** 2327–38
[18] Boero M, Pasquarello A, Sarnthein J and Car R 1997 *Phys. Rev. Lett.* **78** 887–90
[19] Blöchl P E 2000 *Phys. Rev.* B **62** 6158–79
[20] Mysovsky A S, Sushko P V, Mukhopadhyay S, Edwards A H and Shluger A L 2004 *Phys. Rev.* B **69** 085202
[21] Chadi D J 2003 *Appl. Phys. Lett.* **83** 437–9
[22] Griscom D L 2000 *Defects in SiO_2 and Related Dielectrics: Science and Technology* (*NATO Science Series, Series II: Mathematical and Physical Chemistry*) ed G Pacchioni, L Skuja and D L Griscom (Dordrecht: Kluwer) pp 117–60
[23] Lenahan P M and Conley J F Jr 1998 *J. Vac. Sci. Technol.* B **16** 2134–53
[24] Stesmans A, Nouwen B and Afanas'ev V V 2002 *Phys. Rev.* B **66** 045307
[25] Griscom D L and Friebele E J 1986 *Phys. Rev.* B **34** 7524–33
[26] Zhang L and Leisure R G 1996 *J. Appl. Phys.* **80** 3744–9
[27] Chavez J R, Karna S P, Vanheusden K, Brothers C P, Pugh R D, Singaraju B K, Warren W L and Devine R A B 1997 *IEEE Trans. Nucl. Sci.* **44** 1799–803
[28] Tohmon R, Shimogaichi Y, Tsuta Y, Munekuni S, Ohki Y, Hama Y and Nagasawa K 1990 *Phys. Rev.* B **41** 7258–60
[29] Agnello S, Boscaino R, Buscarino G, Cannas M and Gelardi F M 2002 *Phys. Rev.* B **66** 113201
[30] Griscom D L and Cook M 1995 *J. Non-Cryst. Solids* **182** 119–34
[31] Uchino T, Takahashi M and Yoko T 2001 *Phys. Rev. Lett.* **86** 5522–5
[32] Uchino T, Takahashi M and Yoko T 2000 *Phys. Rev.* B **62** 2983
[33] Stirling A and Pasquarello A 2002 *Phys. Rev.* B **66** 245201
[34] Hosono H, Kawazoe H and Matsunami N 1998 *Phys. Rev. Lett.* **80** 317–20
[35] Hosono H and Matsunami N 1998 *Nucl. Instrum. Methods Phys. Res.* B **141** 566–74
[36] Chernov P V, Dianov E M, Karpechev V N, Kornienko L S, Morozova I O, Rybaltovskii A O, Sokolov V O and Sulimov V B 1989 *Phys. Status Solidi* b **156** 663–75
[37] Griscom D L 1992 *J. Non-Cryst. Solids* **149** 137–60
[38] Sasajima Y and Tanimura K 2003 *Phys. Rev.* B **68** 014204
[39] Mukhopadhyay S, Sushko P V, Stoneham A M and Shluger A L 2004 *Phys. Rev.* B **70** 195203
[40] Mukhopadhyay S, Sushko P V, Mashkov V A and Shluger A L 2005 *J. Phys.: Condens. Matter* **17** 1311–8
[41] Nicklaw C J, Lu Z-Y, Fleetwood D M, Schrimpf R D and Pantelides S T 2002 *IEEE Trans. Nucl. Sci.* **49** 2667–73
[42] Mukhopadhyay S, Sushko P V, Edwards A H and Shluger A L 2004 *J. Non-Cryst. Solids* **345/346** 703–9
[43] Nishikawa H, Watanabe E, Ito D and Ohki Y 1994 *J. Non-Cryst. Solids* **179** 179–84
[44] Agnello S, Boscaino R, Gelardi F M and Boizot B 2001 *J. Appl. Phys.* **89** 6002–6
[45] Feigl F J, Fowler W B and Yip K L 1974 *Solid State Commun.* **14** 225–9
[46] Sulimov V B, Sushko P V, Edwards A H, Shluger A L and Stoneham A M 2002 *Phys. Rev.* B **66** 024108
[47] Pacchioni G, Frigoli F, Ricci D and Weil J A 2001 *Phys. Rev.* B **63** 054102
[48] Kunz A B and Klein D L 1978 *Phys. Rev.* B **17** 4614–9

[49] Abarenkov I V, Bulatov V L, Godby R, Heine V, Payne M C, Souchko P V, Titov A V and Tupitsyn I I 1997 *Phys. Rev.* B **56** 1743–50
[50] Kluner T, Govind N, Wang Y A and Carter E A 2002 *J. Chem. Phys.* **116** 42–54
[51] Abarenkov I V and Antonova I M 2004 *Int. J. Quantum Chem.* **100** 649–60
[52] Seijo L and Barandiarán Z 2004 *J. Chem. Phys.* **121** 6698–709
[53] Bacalis N C and Kunz A B 1985 *Phys. Rev.* B **32** 4857–65
[54] Barandiarán Z and Seijo L 1988 *J. Chem. Phys.* **89** 5739–46
[55] Puchin V E, Stefanovich E V and Truong T N 1999 *Chem. Phys. Lett.* **304** 258–64
[56] Todnem K, Børve K J and Nygren M 1999 *Surf. Sci.* **421** 296–307
[57] Hay P J and Wadt W R 1985 *J. Chem. Phys.* **82** 270–83
[58] Wadt W R and Hay P J 1985 *J. Chem. Phys.* **82** 284–98
[59] Dick B G and Overhauser A W 1958 *Phys. Rev.* **112** 90–103
[60] Aguado A, Bernasconi L and Madden P A 2002 *Chem. Phys. Lett.* **356** 437–44
[61] Domene C, Fowler P W, Madden P A, Xu J J, Wheatley R J and Wilson M 2001 *J. Phys. Chem.* A **105** 4136–42
[62] Donnerberg H and Birkholz A 2000 *J. Phys.: Condens. Matter* **12** 8239–47
[63] Nasluzov V A, Ivanova E A, Shor A M, Vayssilov G N, Birkenheuer U and Rösch N 2003 *J. Phys. Chem.* B **107** 2228–41
[64] Sherwood P, de Vries A H, Guest M F, Schreckenbach G, Catlow C R A, French S A, Sokol A A, Bromley S T, Thiel W, Turner A J, Billeter S, Terstegen F, Thiel S, Kendrick J, Rogers S C, Casci J, Watson M, King F, Karlsen E, Sjovoll M, Fahmi A, Schfer A and Lennartz C 2003 *J. Mol. Struct.—Theochem.* **632** 1–28
[65] Sushko P V, Shluger A L and Catlow C R A 2000 *Surf. Sci.* **450** 153–70
[66] Sushko P V, Gavartin J L and Shluger A L 2002 *J. Phys. Chem.* B **106** 2269–76
[67] Johnson M A, Stefanovich E V and Truong T N 1998 *J. Phys. Chem.* B **102** 6391–6
[68] Hess W H, Joly A G, Gerrity D P, Beck K M, Sushko P V and Shluger A L 2001 *J. Chem. Phys.* **115** 9463–72
[69] Braithwaite J S, Sushko P V, Wright K and Catlow C R A 2002 *J. Chem. Phys.* **116** 2628–35
[70] Sushko P V, Shluger A L, Hayashi K, Hirano M and Hosono H 2003 *Phys. Rev. Lett.* **91** 126401
[71] Vollmayr K, Kob W and Binder K 1996 *Phys. Rev.* B **54** 15808–27
[72] Smith W and Forester T R 1996 *J. Mol. Graph.* **14** 136–41
[73] van Beest B W H, Kramer G J and van Santen R A 1990 *Phys. Rev. Lett.* **64** 1955–8
[74] Navrotsky A 1987 *Diffus. Diffus. Data* **53/54** 61
[75] Mott N F and Littleton M J 1938 *Trans. Faraday Soc.* **34** 485–99
[76] Shluger A L, Kotomin E A and Kantorovich L N 1986 *J. Phys. C: Solid State Phys.* **19** 4183–99
[77] Shluger A L and Gale J D 1996 *Phys. Rev.* B **54** 962–9
[78] Pacchioni G, Ieranò G and Márquez A M 1998 *Phys. Rev. Lett.* **81** 377–80
[79] Erbetta D, Ricci D and Pacchioni G 2000 *J. Chem. Phys.* **113** 10744–52
[80] Frisch M J, Trucks G W, Schlegel H B, Scuseria G E, Robb M A, Cheeseman J R, Montgomery J A Jr, Vreven T, Kudin K N, Burant J C, Millam J M, Iyengar S S, Tomasi J, Barone V, Mennucci B, Cossi M, Scalmani G, Rega N, Petersson G A, Nakatsuji H, Hada M, Ehara M, Toyota K, Fukuda R, Hasegawa J, Ishida M, Nakajima T, Honda Y, Kitao O, Nakai H, Klene M, Li X, Knox J E, Hratchian H P, Cross J B, Adamo C, Jaramillo J, Gomperts R, Stratmann R E, Yazyev O, Austin A J, Cammi R, Pomelli C, Ochterski J W, Ayala P Y, Morokuma K, Voth G A, Salvador P, Dannenberg J J, Zakrzewski V G, Dapprich S, Daniels A D, Strain M C, Farkas O, Malick D K, Rabuck A D, Raghavachari K, Foresman J B, Ortiz J V, Cui Q, Baboul A G, Clifford S, Cioslowski J, Stefanov B B, Liu G, Liashenko A, Piskorz P, Komaromi I, Martin R L, Fox D J, Keith T, Al-Laham M A, Peng C Y, Nanayakkara A, Challacombe M, Gill P M W, Johnson B, Chen W, Wong M W, Gonzalez C and Pople J A 2003 *GAUSSIAN 03, Revision B04* (Pittsburgh, PA: Gaussian Inc.)
[81] Reed A E, Weinstock R B and Weinhold F 1985 *J. Chem. Phys.* **83** 735–46
[82] Garvie L A J, Rez P, Alvarez J R, Buseck P R, Craven A J and Brydson R 2000 *Am. Mineral.* **85** 732–8
[83] Trukhin A N and Fitting H J 1999 *J. Non-Cryst. Solids* **248** 49–64
[84] Snyder K C and Fowler W B 1993 *Phys. Rev.* B **48** 13238–43
[85] Stefanov B B and Raghavachari K 1997 *Phys. Rev.* B **56** 5035–8
[86] Pacchioni G and Ieranò G 1997 *Phys. Rev. Lett.* **79** 753–6
[87] Mukhopadhyay S, Sushko P V, Stoneham A M and Shluger A L 2005 *Phys. Rev.* B submitted
[88] Anedda A, Carbonara C M, Corpino R and Serpi A 1999 *J. Non-Cryst. Solids* **245** 183–9
[89] Shluger A and Stefanovich E 1990 *Phys. Rev.* B **42** 9664–73
[90] Griscom D L 1979 *Phys. Rev.* B **20** 1823–34
[91] Tsai T E and Griscom D L 1987 *J. Non-Cryst. Solids* **91** 170–9
[92] Hosono H, Ikuta Y, Kinoshita T, Kajihara K and Hirano M 2001 *Phys. Rev. Lett.* **87** 175501
[93] Itoh N and Stoneham A M 2001 *Materials Modification by Electronic Excitation* (Cambridge: Cambridge University Press)